Title

PHYSICAL PARAMETERS IN EXPOSURE OF LARGE ANIMALS TO HIGH-ENERGY PROTONS

Authors

Sondhaus, Charles A.
Wallace, Roger W.
Lyman, John T.
et al.

Publication Date

1963-09-13

University of California

Ernest O. Lawrence Radiation Laboratory

PHYSICAL PARAMETERS IN EXPOSURE OF LARGE ANIMALS TO HIGH-ENERGY PROTONS

Berkeley, California

DISCLAIMER

IAEA
Conference
Paper No.
SM-44/17
(Part I)

IAEA Symposium in Biological
Effects of Neutron Irradiations
BNL - Oct. 7-11, 1963

UCRL-11015

UNIVERSITY OF CALIFORNIA
Lawrence Radiation Laboratory
Berkeley, California

Contract No. W-7405-eng-48

PHYSICAL PARAMETERS IN EXPOSURE OF LARGE ANIMALS TO HIGH-ENERGY PROTONS

Charles A. Sondhaus, Roger W. Wallace, John T. Lyman,
Kenneth W. Kase, and Palmer G. Steward

September 13, 1963

PHYSICAL PARAMETERS IN EXPOSURE OF LARGE ANIMALS TO HIGH-ENERGY PROTONS

Charles A. Sondhaus, Roger W. Wallace, John T. Lyman, Kenneth W. Kase, and Palmer G. Steward

Donner Laboratory of Biophysics and Medical Physics
University of California, Berkeley, California

September 13, 1963

Abstract

Calculations predict that a beam with intensity profile suitable for large-animal exposures will be produced by multiple Coulomb scattering of the 730-MeV proton beam of the 184-inch cyclotron. Degradation of proton energy to about 50 MeV appears feasible although resulting dose rate may be low. By rotating an animal to simulate omnidirectional exposure, depth-dose patterns similar to those predicted for solar flare proton energy spectra can be produced. Beam intensity and depth dose have been calculated for several proton energies and several diameters of spherical phantom as a preliminary step to experimental study; these results are presented.

PHYSICAL PARAMETERS IN EXPOSURE OF LARGE ANIMALS TO HIGH-ENERGY PROTONS

Charles A. Sondhaus, Roger W. Wallace, John T. Lyman, Kenneth W. Kase, and Palmer G. Steward

Donner Laboratory of Biophysics and Medical Physics
University of California, Berkeley, California

September 13, 1963

1. CHARACTERISTICS AND INTENSITY PROFILE OF A HIGH-ENERGY PROTON BEAM AFTER SCATTERING IN A THICK TARGET

Broad-Beam Exposure of Large Animals

Total-body irradiation of large animals is difficult with the narrow strongly focused proton beam of the 184-inch cyclotron. Attempts have been made to scan large animals by sweeping the exposure holder uniformly through the beam, but mechanical difficulties and stress to the animal have made the technique impractical. In order to produce a total-body irradiation of a large animal without scanning, the first requirement is to enlarge the beam diameter until it exceeds the dimensions of the animal. If an omnidirectional exposure is required to simulate the geometry of solar flare proton exposure, an additional requirement is to present equal portions of the body surface to the beam for equal times at all possible angles by rotating the animal within the broad beam.

Scattering of the beam rather than magnetic deflection was chosen for producing angular divergence. Based on the known properties of the multiple Coulomb scattering process, calculations have been made which predict the angular distribution of the emergent primary proton flux after passage through a scattering target.[1, 2] Substances considered as scatterers include lead, copper, aluminum, and graphite, and the energy range 1000 to 10 MeV has been investigated.

An angular divergence is predicted in the emergent beam which increases with target thickness and is greatest in the heaviest material for a given fraction of particle range. At the same time the intensity of the emergent primary beam within a given small solid angle is reduced because of nuclear interactions that result in secondary particles, mostly protons but including neutrons and mesons, the majority of which are scattered through somewhat larger angles than are the bulk of the multiply scattered primary protons. The resulting reduction in intensity is found to be greatest for the lightest material.

A second effect of the scattering process that has been investigated is the reduction in energy of the emerging particles. The degree of energy degradation in any material is dependent on the fraction of the proton range traversed in the target; this requires a greater thickness of light than of heavy material. Since angular dispersion of the beam is also a function of target thickness, it is evident that neither can be produced without the other. Thus a beam of angular divergence sufficient to irradiate a whole large animal will necessarily consist of lower-energy protons than did the incident beam before striking the target; similarly, a lower-energy beam cannot be used without introducing angular spread and resultant lower intensity. In addition, an energy spread will be produced in the emergent primary beam which will increase with target thickness; this energy straggling, however, remains a small percent of the emergent energy until very low degraded energies are reached, of about 10 to 50 MeV, at which region it becomes comparable.

Calculation of Beam Intensity Profile

In order to determine the intensity profile of a proton beam degraded by scattering, calculations based on the analysis of a variable-energy beam for the proposed NASA synchrocyclotron[1] have been extended to the broad-beam case for biological use.[2] The degraded beam will be analyzed experimentally.

The initial beam was assumed to be a thin pencil of monoenergetic 730-MeV protons. This initial beam was then assumed to be degraded in a carbon or copper scatterer to some final energy. The beam profile at some given distance from the scatterer was calculated by using circular Gaussian error probabilities,[3] and the remanent intensity was then determined.

According to circular error probability, if a set of points is distributed normally in two dimensions with equal standard deviations, the probability that a point will fall within a distance r of the mean (or a distance r from the center of the circle in this case) is $1 - \exp(-K^2/2)$, where $K = r/\sigma$ and σ is one standard deviation. In the case under discussion, the scattering was in terms of a root-mean-square scattering angle ϕ_a; and so K was expressed as $\frac{r}{d}/\phi_a$, where d is the distance from the scatterer to the target.

The beam profile is thus dependent upon both the rms scattering angle ϕ_a and the distance from the scatterer to the target d. The angle ϕ_a is in turn dependent upon the scattering material and the energy to which the beam is degraded.

The first step in the procedure is to choose a scattering material and a degraded energy. From this a ϕ_a is determined. It is then assumed that the beam emerges from the scatterer at a point and diverges with a circular intensity cross section. A scatterer-to-target distance is chosen and the K's are then calculated as a function of perpendicular distance from the beam axis across the beam cross section. The calculations were usually done in 1-cm increments from the center of the beam to about 20 cm radius.

From the values of K, the probability that a proton will strike within a circle of radius $K\phi_a d$ about the center of the beam is next calculated. The beam cross section is then divided into circular rings 1 cm thick, and the probability that a proton will strike within each ring is calculated by

$\Delta P = [1 - \exp(-K_2/2)] - [1 - \exp(-K_1/2)]$; where K_1 and K_2 correspond to two successive radii.

The remanent intensity is found by applying a remanent intensity factor f based on the degree of energy degradation and the scattering material.[2] This factor describes the primary beam attenuation in the scatterer. The flux profile of the degraded beam is then found in terms of protons/cm^2-sec by multiplying the initial intensity I by the probability ΔP that a proton will strike in a given ring and dividing by the area of the ring, A:

$$\Phi = I\Delta P/A.$$

It should be noted that these calculations do not take into consideration the fact that the beam is spread somewhat in the scatterer and is thus subject to a radial as well as angular divergence. However, the correction required by the radial spreading within the scatterer is small; moreover, it serves to flatten the profile and hence improve the picture.

Expected Intensities after Degradation in Graphite and Copper

These calculations allow predictions of the energy and intensity profile of the primary beam emerging from a target of each of the above materials. It appears that intensity can be made sensibly uniform over a circular area of more than 30 cm diameter at a sufficient distance from the scattering-target exit port. Some representative results are seen in Fig. 1, which shows profiles produced by degradation in graphite to energies of 400, 200, and 100 M
It is seen that distribution is uniform over this diameter at a distance of 3 to 5 meters, if a graphite target is used with thickness great enough to degrade the initial energy of 730 MeV to roughly 400 MeV. The resulting primary flux intensity appears to be reduced by a factor of between 100 and 1000, suggesting that the maximum dose rate achievable in air in the target region may lie in

the range of 10 to 100 rad/min. Different profiles and intensities are obtained for other scattering materials and other distances between scatterer and target at the same degraded beam energy. In general the more the energy is degraded, the more the beam is spread, so that a uniform field over a large area can be found at shorter scatterer-to-target distances for larger energy degradations in thicker targets. A copper scatterer spreads the beam more than does a carbon scatterer and so produces a more uniform intensity over a given area at a given scatterer-to-target distance. However, a copper scatterer also results in a much smaller remanent flux intensity than does carbon for a given energy degradation.

Figure 2 shows profiles produced by degradation in copper to 400, 200, and 100 MeV. It is seen that if a 100-MeV beam is desired, the same area of roughly uniform intensity can be found at a distance of 1 meter from a copper target, and dose rate due to the primary beam may be kept to about the same value as above.

Since secondary-particle production also occurs in the scattering target and some fraction of the secondary-particle flux also reaches the animal, calculations are under way to estimate the increase in dose due to this component; the total flux will be determined experimentally. The theory predicts that the secondary-particle flux will be smallest in graphite. For this reason as well as the higher remanent intensity predicted for graphite, this material has been chosen for the primary beam-scattering target for whole-body irradiation of large animals at high energy with the 184-inch cyclotron. It appears that a second target of copper following the graphite target will be optimal in producing a lower-energy broad beam while conserving the most intensity. Thus, a 400-MeV exposure at 3 to 5 meters from a 58-cm-thick graphite target should produce uniform dose distribution in a large animal, while exposures at 100 MeV and

below appear feasible at 1 meter from the graphite target when an additional target of copper 12 cm or more thick is added. Alternatively, a copper target alone 32 cm or more thick might be substituted for the graphite.

It appears from these calculations and those for depth dose that the stepwise simulation of a solar flare proton exposure in the lethal dose range[4] would be possible by using as few as three proton energies--e.g., 50, 100, and 400 MeV in the intensity ratio 5:2:1--such as to produce a midline dose in the order of 200 to 400 rad. It appears that this would require very roughly a 10-min exposure to 400-MeV protons, a 20-min exposure to 100-MeV protons and a 2- to 4-hour exposure to 50-MeV protons if the scattering targets discussed here are used. To produce the lowest-energy proton dose in the outer 2 cm of tissue appears to be the most time-consuming step. Rotating the animal in the 88-inch cyclotron beam may be a logical procedure for this part of the exposure. For the production of a uniform total-body proton dose in a large animal, however, the scattering technique appears to lead to reasonable exposure times at fairly high energies.

2. DEPTH DOSE IN LARGE PHANTOMS IRRADIATED OMNIDIRECTIONALLY WITH HIGH-ENERGY PROTONS

Factors Influencing Dose Distribution

In evaluating the effect of a total-body exposure of a large animal to a radiation flux, it is of considerable importance to know the distribution of tissue dose and of LET at various depths in the animal.[5,6] Both quantities appear to be essentially constant at all points even in a large animal exposed to protons if the proton energy is sufficiently high; two factors may produce deviations from uniformity, however. The first is the attenuation of the primary beam and the production of secondary particles by the interaction of primary protons with nuclei of atoms in the tissue. The second is the scattering

and energy degradation of the primary proton flux by multiple Coulomb interactions in passage through the material. The relative importance of each process varies with the energy of the incident proton flux as well as with the size of the animal.

A number of calculations have been made by different investigators in attempting to predict the behavior of dose and LET with depth for the case in which the proton flux is distributed in energy and is isotropically incident.[4,7,8] (Present information indicates that these are the conditions under which an exposure to a solar-flare proton flux might occur during the course of a space flight.) The numerical values of dose and the shapes of the depth-dose profiles resulting from such estimates differ somewhat according to the varying assumptions made in each investigation; the problem is a complex one and detailed information on nuclear interactions and secondary particle production is scarce. Furthermore the energy spectrum of the solar-flare proton flux appears to vary greatly among different events and at different times during a given event,[9] making the predicted values somewhat arbitrary.

In an experimental approach to this problem, lucite phantoms will be exposed to the protons from the 184-inch cyclotron after the beam has passed through a scattering target which produces energy degradation and angular divergence in the emergent broad beam. Dose will be measured at a series of radial depths inward from the surface of a test sphere, and in tissue-equivalent animal phantoms, by means of fluorescence readings in silver-activated phosphate glass dosimeters as well as with lithium fluoride thermoluminescent dosimeters.

As a preliminary phase of these experiments, a series of calculations have been programmed for the 7090 computer at Lawrence Radiation Laboratory to predict approximately the dose, particle energy, and LET distribution in an omnidirectionally irradiated spherical phantom as a function of incident

primary particle energy and of sphere diameter. The program was designed to allow the imput of any chosen value for each of the parameters involved, so that improvement resulting from further experimental determinations may easily be incorporated into the computations.

Calculation of Proton Dose

The program of computation was divided into two parts. The first was the calculation of dose at given depth due to the primary proton flux alone. Geometric differences in path length with angle of entry through a sphere lead to a distribution of energy in the primary proton flux arriving at each dose point The percent of total dose contributed by protons in each of several energy intervals has therefore been tabulated, and the sum of the partial doses then forms the total dose due to the primaries. A value of dE/dx and thus of average LET can be assigned to each energy, resulting in an estimate of average LET distribution at each point.

The second part of the computation is a recalculation of dose at each point to include the contribution of three classes of interactions producing secondary particles; the nuclear cascades, the evaporation events, and the elastic interactions with hydrogen. By assuming rough energy distributions for each and by carrying the cascade and elastically scattered proton secondarie through successive depths, a total additional dose due to each type of interaction at each depth point chosen can also be roughly broken down into energy intervals and added to the primary dose distribution. These calculations are in progress. Meson and neutron doses are not considered in the present program.

The first part of the calculation (the contribution from only the primary proton flux) has been developed into an operating computer code, which may be described briefly as follows.

The number of protons per sec, dn, reaching a test mass of volume dA·dr (see Fig. 3) from an incremental area $d\sigma$ on the surface of a sphere is given by

$$dn = \frac{\Phi}{4\pi} \, d\omega \cos\alpha \, d\sigma, \qquad (1)$$

where Φ = isotropic flux at $d\sigma$,

$d\omega = \frac{dA}{R_1(\theta)^2}$ = solid angle subtended by dA at distance $R_1(\theta)$ from $d\sigma$,

$d\sigma = 2\pi r_0^2 \sin\theta d\theta$ = elemental surface area on sphere,

$$\cos\alpha = \frac{r_0^2 + R_1^2(\theta) - (r_0-d)^2}{2 r_0 R_1(\theta)} \quad \text{(law of cosines)},$$

r_0 = sphere radius, and

d = depth of test mass in sphere.

To allow approximately for the contribution of secondaries, the attenuation due to interaction between the sphere material and the incident protons is neglected.

The dose rate, dD, produced in this same test mass due to the protons per sec reaching the dose point from the surface area $d\sigma$ is

$$dD = \left(\frac{dE}{dr}\right)_E \frac{dr}{dm} \, dn = \left(\frac{dE}{dr}\right)_E \cdot \left(\frac{dr}{\rho \, dA \, dr}\right) dn, \qquad (2)$$

where

$\left(\frac{dE}{dr}\right)_E$ = the stopping power for a proton of energy E in tissue,

dm = mass of test volume, and

ρ = density of test mass (1.0 for tissue).

Combining the above expressions and letting $\mu = \cos\theta$, we have

$$R^2(\theta) = r_0^2 + (r_0 - d)^2 - 2 r_0 (r_0 - d)\mu$$

and thus

$$dD = \frac{\Phi}{2} \frac{r_0^2}{\rho} \left(\frac{dE}{dr}\right)_E \cdot \frac{(r_0 - (r_0-d)\mu)d\mu}{[r_0^2 + (r_0-d)^2 - 2 r_0 (r_0-d)\mu]^{3/2}}. \qquad (3)$$

To obtain an analytical expression for $\frac{dE}{dr}$, we break the range-energy curve for protons in tissue into five straight-line segments on log-log graph paper, for each of which $R = p\,E^q$, where

R = residual range of the proton in tissue,

E = proton energy,

and p and q represent the intercept and slope respectively on log-log graph paper.

Note that if we let the variable E equal the proton energy at the dose point, and the constant E_0 equal the incident proton energy, then

$$R_1(\theta) = p\,E_0^q - pE^q.$$

Choosing the variable E in preference to μ,

$$dD = \frac{\Phi}{4\rho}\,\frac{1}{(r_0-d)}\left[\frac{r_0^2-(r_0-d)^2}{(pE_0^q-pE^q)^2}+1\right]dE,$$

so that

$$D = \frac{\Phi}{4\rho}\,\frac{1}{(r_0-d)}\int_{E_{min}}^{E_{max}}\left[\frac{r_0^2-(r_0-d)^2}{(pE_0^q-pE^q)^2}+1\right]dE. \qquad (4)$$

Here,

$$E_{max} = \left(\frac{pE_0^q-d}{p}\right)^{1/q} \quad \text{for } pE_0^q - d > 0,$$

$$E_{min} = \left(\frac{pE_0^q - r_0-(r_0-d)}{p}\right)^{1/q} \quad \text{for } pE_0^q - r_0 - (r_0-d) > 0,$$

where E_{min} = minimum energy of protons reaching test mass,

E_{max} = maximum energy of protons reaching test mass,

r_0 = radius of the sphere,

d = depth in the sphere at which data are desired.

The computer code performs a numerical integration of Eq. (4) by the application of Simpson's rule. This expression of the total dose rate results in an extremely rapid calculation, each dose point requiring about 0.5 sec for a given incident proton energy. For calculation of dose at 10 depths in each of six sphere diameters for protons of 6 to 10 different incident energies, the total computer time required was less than 3 minutes.

The following assumptions are implicit in the code:

1. The range-energy curve is broken into five segments, each of them represented by a function of the form

$$R = p_i E^{qi} \quad \text{for } 1 \leq i \leq 5 .$$

2. The only interaction considered between the protons and the sphere is ionization energy loss.

3. The effects of straggling are neglected; i.e., all protons of a given initial energy are assumed to reach peak ionization density at exactly the same path length.

For the second part of the calculation, a code is being developed which attempts to include removal of primary protons by nuclear collision and the contribution of secondary particles to the dose. Three types of secondaries are considered:

1. Cascade protons resulting from inelastic collisions between primary protons and nuclei in the sphere.

2. Evaporation protons resulting from inelastic interaction between primary protons and nuclei in the sphere.

3. Recoiling hydrogen atoms and scattered primary protons resulting from elastic scattering of the primary protons on hydrogen atoms in the sphere. Only first-generation secondaries are being considered.

The energy spectrum of the cascade proton secondaries is represented by a power function, and it is assumed that they are all emitted in the forward direction (i. e., the secondary continues on in the direction of the incident primary).

The evaporation protons are assumed to have a Maxwellian energy distribution. Owing to their low energy, it is assumed that all their energy is deposited at the point of formation.

The energy spectrum of recoiling hydrogen nuclei and scattered primary protons is calculated from the application of conservation of energy and momentum to the p-p differential elastic scattering cross section. It is assumed that both the recoil hydrogen nuclei and the scattered incident protons are emitted in the forward direction with the energy calculated by the method indicated above.

Results and Discussion

The output of the initial computer program is in the form of depth-dose data and fraction of dose due to protons in each of several energy intervals at each dose point in the sphere; average LET distribution is calculable from the latter at each depth. These data have been calculated for tissue-equivalent spheres of diameter 5 to 100 cm, exposed omnidirectionally to monoenergetic proton fluxes of energy between 20 and 730 MeV. The curves of depth dose for the 30-cm-diameter sphere are essentially flat down to about 200 MeV, indicating that uniform whole-body exposure of large animals is possible at this energy or higher. Below this energy region the ratio of surface to midline dose increases rapidly with decreasing energy and increasing sphere diameter, the midline dose from primaries alone becoming zero at the lowest energies considered.

Some results available from the first code (primary proton flux only) are presented in Figs. 4 through 7 and in Table I. In Fig. 4, depth-dose curves are shown for several proton energies incident on a sphere of tissue of 10 cm diameter. A pronounced peak dose occurs at 4 cm depth for 80-MeV protons. This peak is unusually high because all incident protons of 80 MeV that approach the center of the sphere reach the end of their range and therefore deposit their maximum energy density in a region of the sphere near its midpoint, resulting in a large $\frac{dE}{dx}$ contribution from all directions. The peak at 1 cm depth for 100-MeV protons is caused by the Bragg peak of protons that enter the sphere from directions resulting in a path length in the sphere of approximately 9 cm. Protons with initial energy 150 MeV and higher produce an approximately flat depth-dose curve in the 10-cm sphere.

Figure 5 shows similar curves for a 20-cm-diameter sphere, roughly equal in volume to a small primate. For this sphere, protons of energy 200 MeV and above produce an essentially flat depth-dose curve. Protons of about 110 MeV cause a pronounced peak near the center of the sphere, as seen in the figure.

Protons of 140 MeV cause the corresponding peak in the 30-cm-diameter sphere (Fig. 6). For 200-MeV protons the beginning of a peak is seen near the surface of the sphere. Similar cases occur at certain proton energies for any sphere diameter.

A consequence of this depth-dose pattern is that in uniform exposure by rotation, approaching the omnidirectional case, a Bragg ionization peak at depth d cannot be produced by irradiating with monoenergetic protons of range d, since the smearing out of ionization peaks by the rotation produces a continuously decreasing dose distribution with depth. Instead, protons with energy such as to cross the sphere with range $(2\ r_0 - d)$ must be used, where

r_0 is the radius of the spherical tissue volume. Therefore the center of the sphere and all other points within it always receive some dose, although smaller than the Bragg peak dose.

Table I is an example of the information the code computes; which is intended to make possible the calculation of average LET versus depth for any incident proton energy. The specific data tabulated are for a 30-cm-diameter sphere exposed omnidirectionally to a flux of 150-MeV protons. The large contribution to the dose of the low-energy protons at 12 cm depth is shown in Fig. 6; about 75% of this dose is contributed by protons of energy between 20 and 80 MeV with an LET distribution of average value about 1.5 to 2 keV/μ. About 5% of the 12-cm-depth dose is contributed by protons of 5 MeV and less, with average LET about 20 keV/μ.

Table II gives an idealized solar flare energy spectrum[6] which was used together with Fig. 6 to calculate a depth-dose curve for a 30-cm-diameter sphere of tissue. The result is shown in Fig. 7, which is in general agreement with this particular case as treated elsewhere.[2, 3] A large surface dose is contributed by the low-energy flare protons in an unshielded sphere. The effect of shielding may be estimated by recognizing that, for example, the curve remaining from 1 to 15 cm depth represents a depth-dose curve in a sphere of 28 cm diameter shielded by 1 cm of water. The depth-dose distribution for this solar flare case would be fairly well duplicated by an exposure to 50-, 100-, and 400-MeV protons in the intensity ratio 5:2:1.

The dose distribution in a sphere exposed to any arbitrary solar proton spectrum may be similarly obtained from this computer code by summing the contributions from each energy interval in an assumed spectral distribution. If the dose distribution predicted for a test sphere is reproduced experimentally,

the proper exposure times and proton energies at the 184-inch cyclotron can be chosen to simulate the solar flare condition to a degree sufficient for animal irradiation. A large animal rotator, shown in Fig. 8, has been constructed for use in the large-animal, total-body omnidirectional exposures, and experimental dose determinations to confirm the predicted distributions will be made with the phantom or test sphere placed within it. Sinusoidal motion around the vertical axis combined with uniform rotation horizontally will be used to generate an approximately isotropic flux geometry.

Acknowledgments

We wish to express our appreciation to Dr. John H. Lawrence and Dr. Cornelius A. Tobias for their interest and support, and to Mrs. Barbara Levine for her assistance in programming and performing the calculations on the 7090 computer.

These studies are funded by the National Aeronautics and Space Administration through the Atomic Energy Commission and the Lawrence Radiation Laboratory.

References

1. B. J. Moyer, Beam Characteristics of 600-MeV Synchrocyclotron; Appendix II of NASA Report No.200-90-1-R3 (W. Brobeck and associates).
2. C. A. Sondhaus and R. W. Wallace, Solar Proton Exposure Simulation with the 184-Inch Cyclotron, UCRL-10447, Nov. 1962 (unpublished).
3. H. L. Harter, Circular Error Probability, J. Am. Stat. Assoc. 55, 292 (Dec. 1960).
4. Proceedings of the Symposium on Protection Against Radiation Hazards in Space, Gatlinburg, Tenn., Nov. 1962, TID-7652.
5. V. P. Bond, R. E. Carter, J. S. Robertson, P. H. Seymour, and H. H. Hechter, The Effects of Total Body Fast Neutron Irradiation of Dogs, Rad. Res. 4, 139 (1956).
6. V. P. Bond, E. P. Cronkite, C. A. Sondhaus, G. W. Imrie, J. S. Robertson, and D. C. Borg, The Influence of Exposure Geometry on the Pattern of Radiation Dose Delivered to Large Animal Phantoms, Rad. Res. 6, 554 (1957).
7. R. D. Evans, Principles for the Calculation of Radiation Dose Rates in Space Vehicles; Technical Report to the N.A.S.A., A. D. Little Co. Report 63270-05-01, July 1961.
8. H. J. Schaefer, Tissue Ionization Dosages in Proton Radiation Fields in Space; Aerospace Med. 31, 807-816 (1960); also, this conference, paper SM-44/30.
9. D. K. Bailey, Time Variations of the Energy Spectrum of Solar Cosmic Rays in Relation to the Radiation Hazard in Space, J. Geophys. Res. 37, 391 (1962).

Table I. Depth-dose data for 150-MeV protons incident upon the 30-cm-diameter sphere of tissue-equivalent material.

Depth (cm)	Total dose rate (rad/h) / 10^6 proton/cm^2-sec	Dose rate per energy interval						
		0-5	5-10	10-20	20-40	40-80	80-150	Energy interval(MeV)
		~ 20	6.0	3.7	2.2	1.2	~ 0.7	LET (keV/μ)
0.2	285	4.95	4.95	9.89	19.8	40.0	205.	
0.5	290	5.19	5.19	10.4	20.9	42.6	206.	
1.0	299	5.59	5.59	11.2	22.6	47.1	207.	
1.5	307	6.05	6.05	12.1	24.5	51.8	207.	
2.0	315	6.50	6.50	13.0	26.5	56.7	206.	
3.0	331	7.50	7.50	15.1	30.7	67.2	203.	
6.0	387	11.5	11.5	23.4	48.1	100.	192.	
9.0	481	19.0	19.0	38.4	79.5	186.	138.	
12.0	724	32.0	40.0	81.1	168.	398.	4.72	
15.0	590	0	0	0	0	590	0	

Table II. An idealized (omnidirectional flux) solar-flare proton energy spectrum - 16 hours after onset of the radiation surge. (Data from reference 6.)

Energy group (MeV)	Proton group (cm^2-sec)
15-25	2.52×10^4
25-35	1.01×10^4
35-45	5.03×10^3
45-70	7.16×10^3
70-125	3.17×10^3
125-175	7.41×10^2
175-225	1.76×10^2
225- ∞	6.29×10^1

Figure Legends

Fig. 1. Beam intensity profiles produced by degradation of 730-MeV protons in graphite to energies of 400, 200, and 100 MeV.

Fig. 2. Beam intensity profiles produced by degradation of 730-MeV protons in copper to energies of 400, 200, and 100 MeV.

Fig. 3. Geometrical representation of a proton beam element entering the sphere of the radius r_0 through $d\sigma$, spreading into the solid angle $d\omega$ about $R_1(\theta)$, and striking the test volume $dr \cdot dA$ at depth d in the sphere.

Fig. 4. Dose rate produced by an isotropic proton flux upon a 10-cm-diameter sphere of tissue-equivalent material (primary proton contribution only).

Fig. 5. Dose rate produced by an isotropic proton flux upon a 20-cm-diameter sphere of tissue-equivalent material (primary proton contribution only).

Fig. 6. Dose rate produced by an isotropic proton flux upon a 30-cm-diameter sphere of tissue-equivalent material (primary proton contribution only).

Fig. 7. Depth-dose rate curves for a 30-cm-diameter sphere of tissue, using Bailey's idealized energy spectrum of solar protons--16 hours after onset of the radiation surge.

Fig. 8. Large animal omnidirectional rotator.

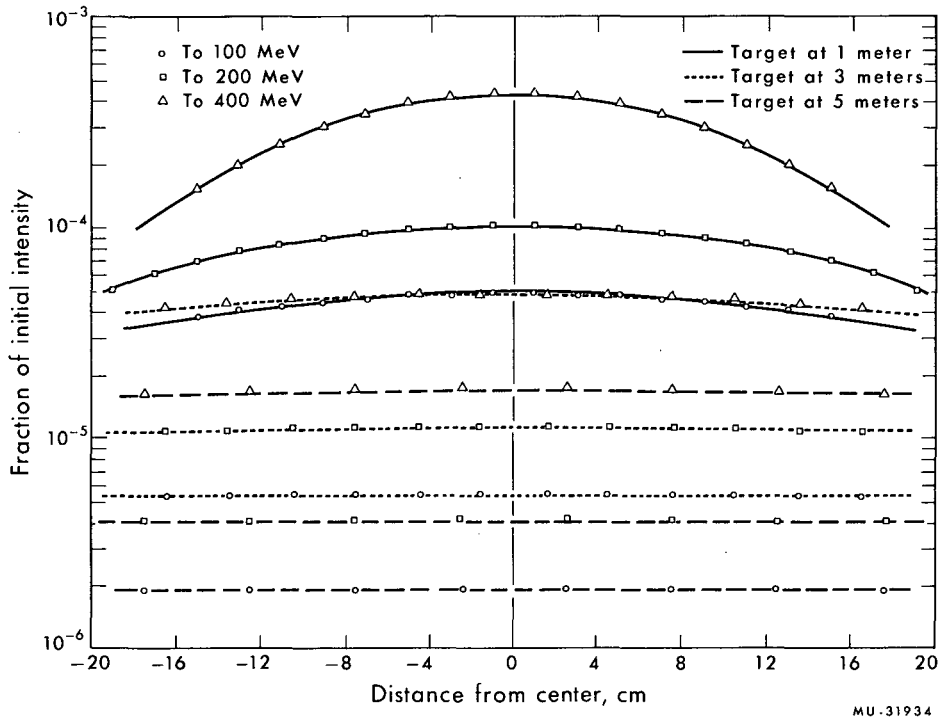
o To 100 MeV
□ To 200 MeV
△ To 400 MeV
Target at 1 meter
Target at 3 meters
Target at 5 meters
Fraction of initial intensity
10^{-3}
10^{-4}
10^{-5}
10^{-6}
−20 −16 −12 −8 −4 0 4 8 12 16 20
Distance from center, cm
MU-31934

Fig. 1.

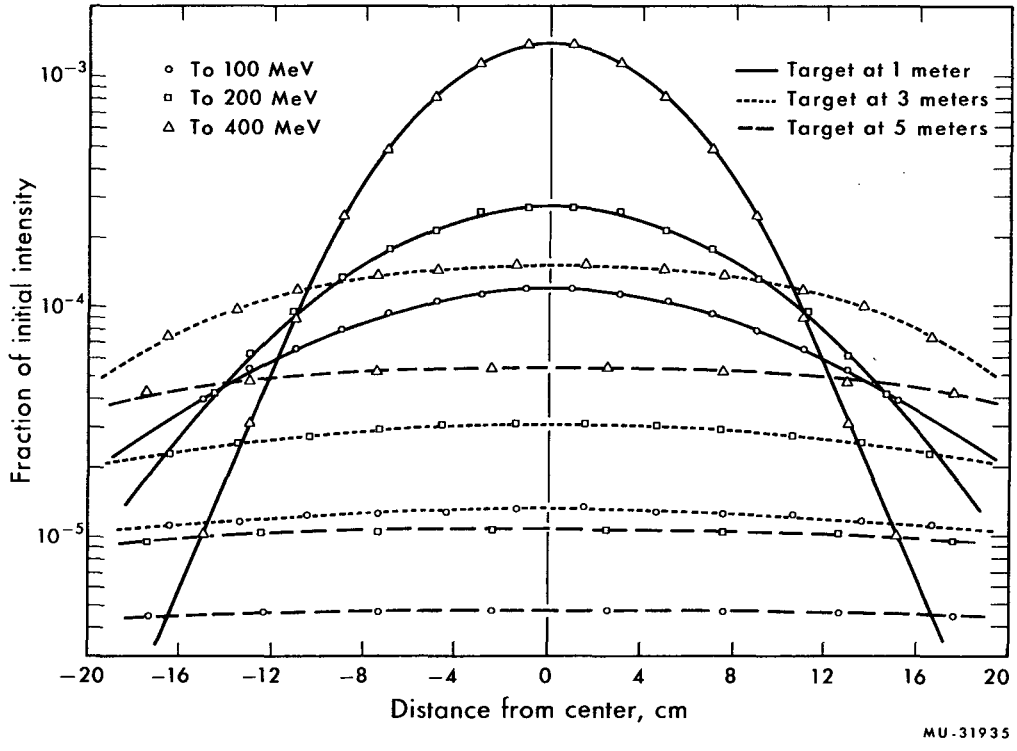
To 100 MeV
To 200 MeV
To 400 MeV
Target at 1 meter
Target at 3 meters
Target at 5 meters
Fraction of initial intensity
10^{-3}
10^{-4}
10^{-5}
−20
−16
−12
−8
−4
0
4
8
12
16
20
Distance from center, cm
MU-31935

Fig. 2.

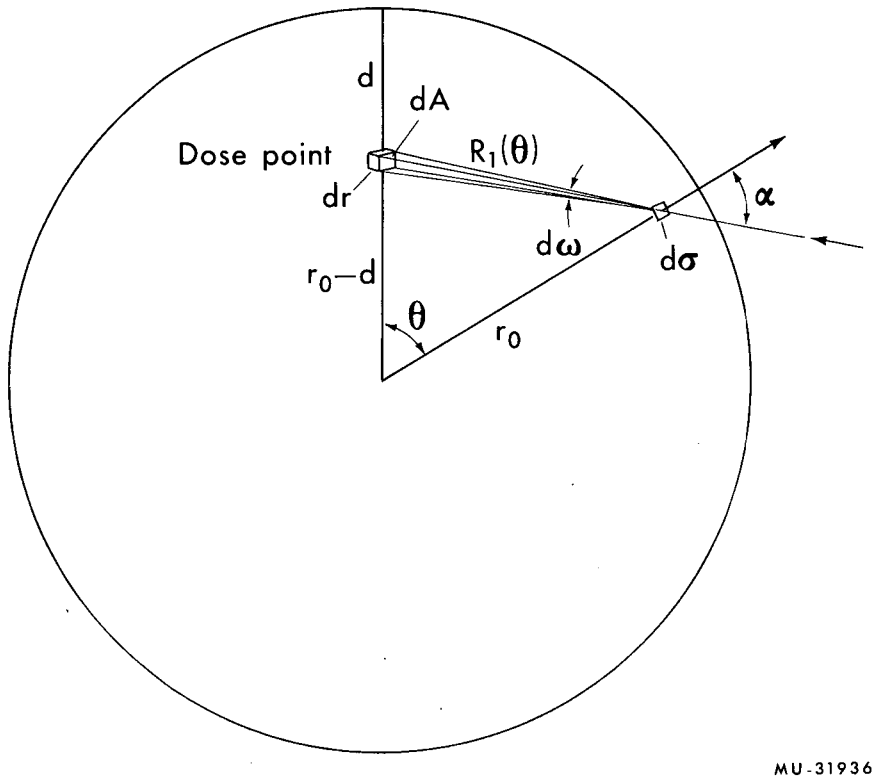
d
dA
Dose point
$R_1(\theta)$
dr
α
$d\omega$
$d\sigma$
r_0-d
θ
r_0
MU-31936

Fig. 3.

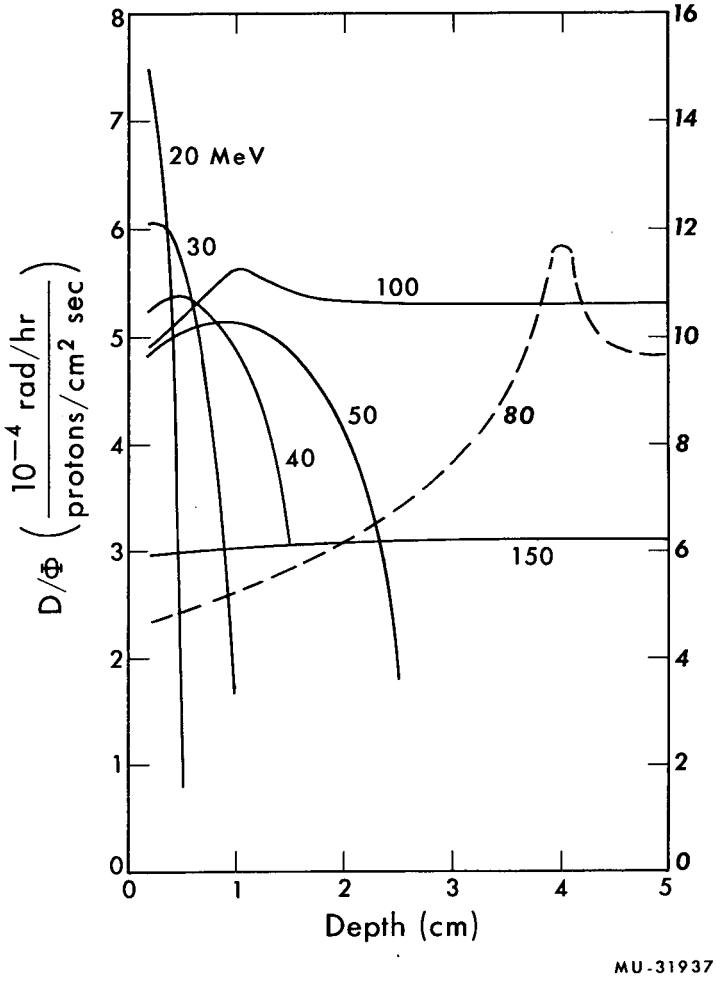
20 MeV
30
100
50
40
80
150
D/Φ ($\frac{10^{-4}\ \text{rad/hr}}{\text{protons/cm}^2\ \text{sec}}$)
Depth (cm)
0
1
2
3
4
5
6
7
8
10
12
14
16
MU-31937

Fig. 4.

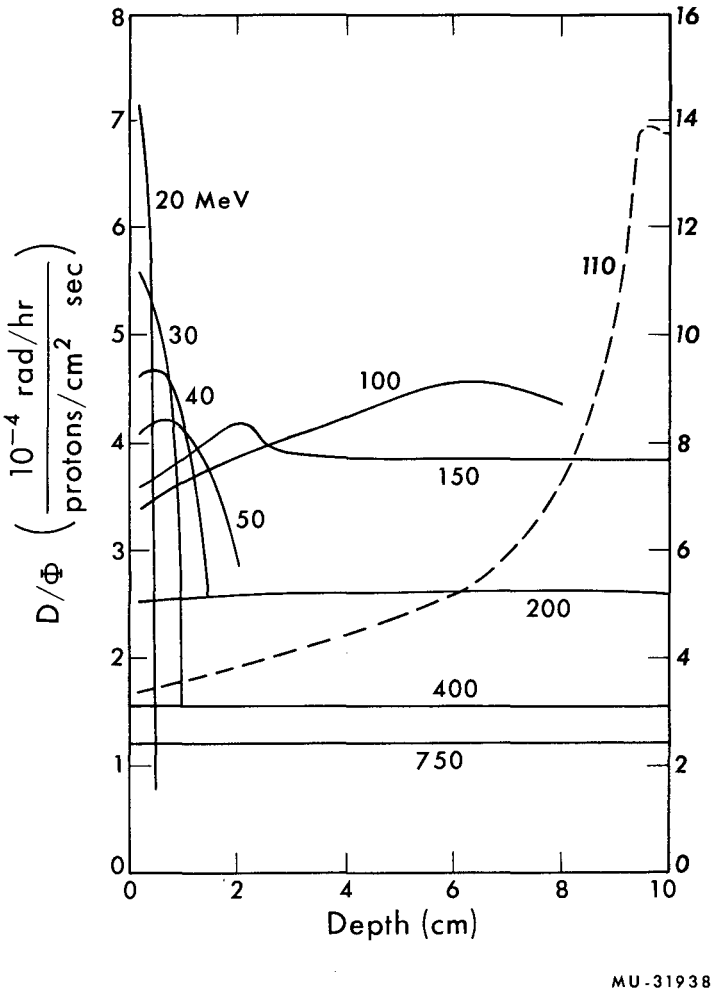
D/Φ (10⁻⁴ rad/hr / protons/cm² sec)
Depth (cm)
20 MeV
30
40
50
100
110
150
200
400
750
MU-31938

Fig. 5.

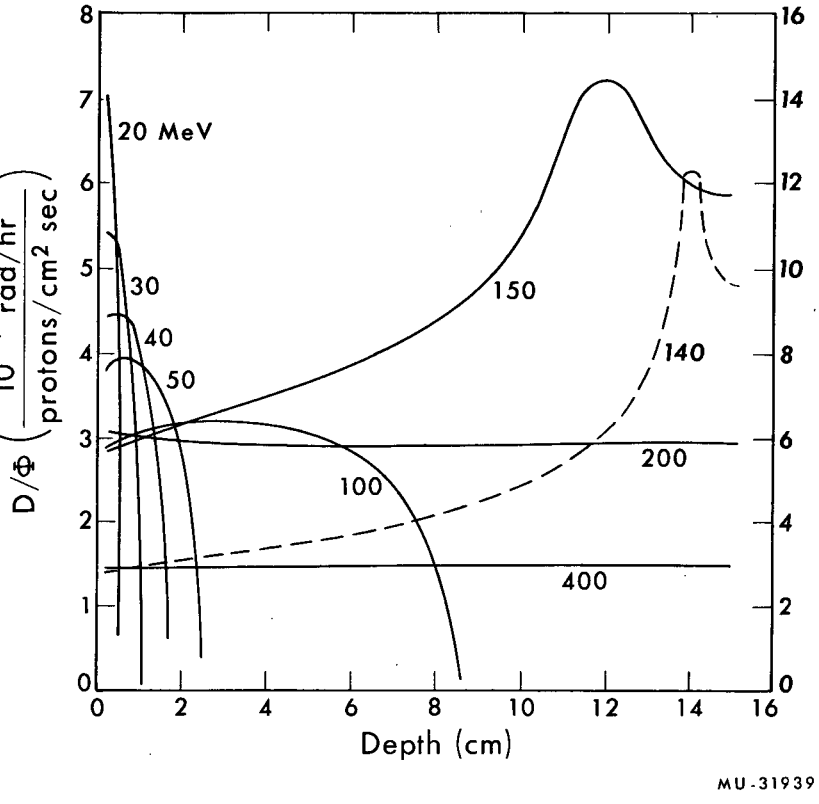
20 MeV
30
40
50
100
150
140
200
400
Depth (cm)
D/Φ (10⁻⁴ rad/hr / protons/cm² sec)
MU-31939

Fig. 6.

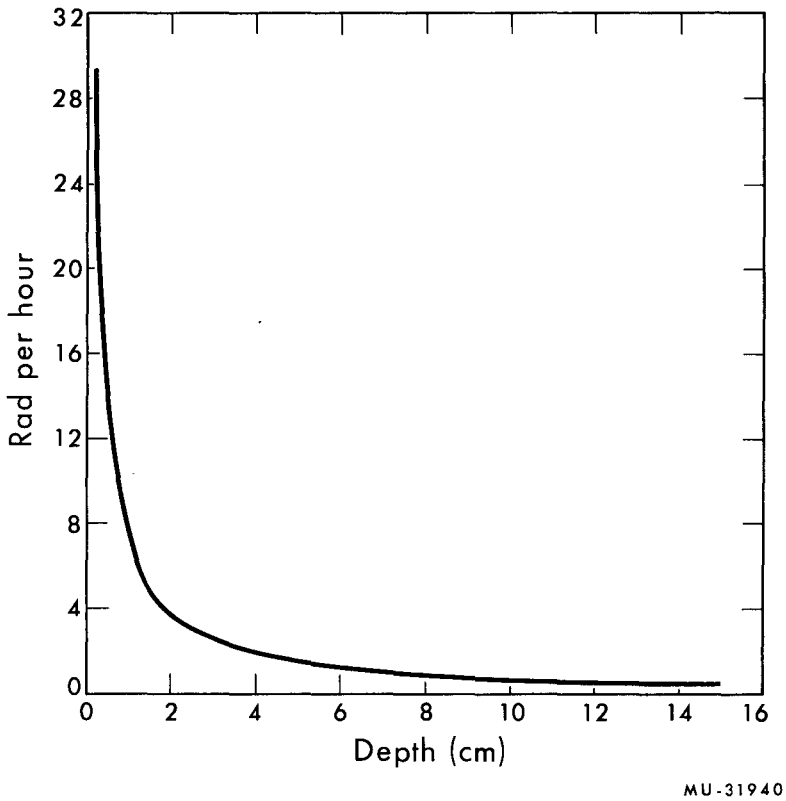
32
28
24
20
16
12
8
4
0
Rad per hour
0
2
4
6
8
10
12
14
16
Depth (cm)
MU-31940

Fig. 7.

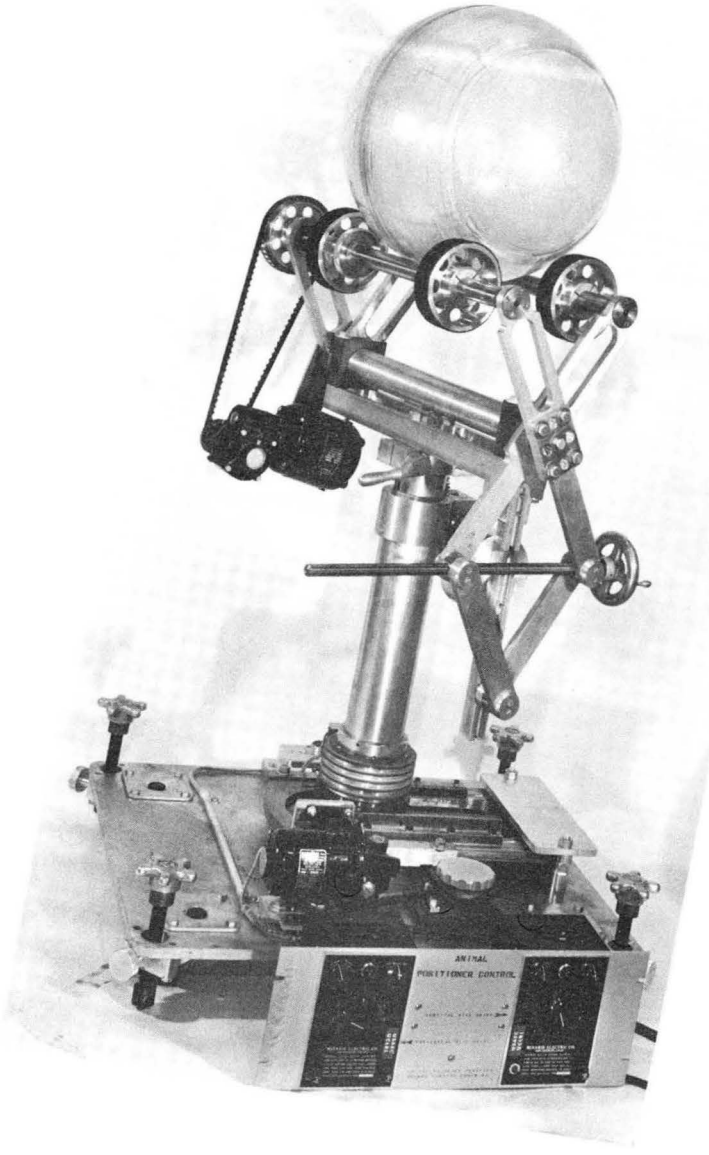

ZN-3941

Fig. 8.